HHS Public Access

Author manuscript

Ultrasound Med Biol. Author manuscript; available in PMC 2024 May 01.

Published in final edited form as:

Ultrasound Med Biol. 2023 May ; 49(5): 1082–1090. doi:10.1016/j.ultrasmedbio.2022.12.006.

Molecular Identity Changes of Tumor-Associated Macrophages and Microglia after MRgFUS induced BBB Opening in a Mouse Glioblastoma Model

Yanrong Zhang, MD, PhD[1], **Jing Wang, MD**[1,2], **Sara Natasha Ghobadi, BS**[1], **Haiyan Zhou, MD**[1,3], **Ai Huang, MD**[1,4], **Marco Gerosa, PhD**[1,5], **Qingyi Hou, MD**[1,6], **Olivier Keunen, PhD**[7], **Anna Golebiewska, PhD**[8], **Frezghi G. Habte, PhD**[9], **Gerald A. Grant, MD**[10], **Ramasamy Paulmurugan, PhD**[11], **Kevin S. Lee, PhD**[12], **Max Wintermark, MD**[13]

[1]Department of Radiology, Neuroradiology Division, Stanford University, CA, USA

[2]Department of Radiology, Shandong Provincial Hospital Affiliated to Shandong First Medical University,324 Jing-wu Road, Jinan 250021, China

[3]The Acupuncture and Tuina School/Third Teaching Hospital, Chengdu University of Traditional Chinese Medicine, Chengdu, Sichuan, China

[4]Cancer Center, Union Hospital, Tongji Medical College, Huazhong University of Science and Technology, Wuhan 430022, China

[5]Department of Diagnostic and Public Health, University of Verona, Verona, Italy, 37135

[6]Department of Nuclear Medicine, Guangdong Provincial People's Hospital, Guangzhou 510080, China

[7]In Vivo Imaging Facility, Luxembourg Institute of Health, 84 Val Fleuri, L-1526 Luxembourg

[8]Department of Oncology, Luxembourg Institute of Health, 84, Val Fleuri, L-1526 Luxembourg

[9]Department of Radiology, Molecular Imaging Program at Stanford, CA, USA

Corresponding author: Max Wintermark, MD, University of Texas MD Anderson, Department of Neuroradiology, 1400 Pressler Street, Unit 1482, Houston, TX 77030-4009, Phone number: (713)792-0485, Max.Wintermark@gmail.com.
Co-Senior Authors: Max Wintermark, MD, University of Texas MD Anderson, Department of Neuroradiology, 1400 Pressler Street, Unit 1482, Houston, TX 77030-4009; Kevin S. Lee, PhD, Department of Neuroscience, University of Virginia School of Medicine, Charlottesville,, VA 22901.

Authors' contributions

Conception and design: Lee, Wintermark. Animal model: Ghobadi, Zhou. MRI technical support: Keunen, Habte. Acquisition of data: Zhang, Wang, Ghobadi, Zhou, Huang, Hou, Keunen. Analysis and interpretation of data: Zhang, Gerosa, Keunen, Golebiewska. Drafting the article: Zhang. Critically revising the article: Zhang, Keunen, Golebiewska, Paulmurugan, Lee, Wintermark. Reviewed submitted version of manuscript: Zhang, Grant, Paulmurugan, Lee,Wintermark. Approved the final version of the manuscript on behalf of all authors: Wintermark.

Conflict of interest disclosure

The authors report no conflict of interest.

Research data for this article

Raw data would remain confidential and would not be shared.

[10]Division of Pediatric Neurosurgery, Department of Neurosurgery, Lucile Packard Children's Hospital, Stanford University School of Medicine, Stanford, CA, USA.

[11]Molecular Imaging Program at Stanford (MIPS), Canary Center for Cancer Early Detection, Department of Radiology, Stanford University, CA, USA

[12]Departments of Neuroscience and Neurosurgery, and Center for Brain, Immunology, and Glia, School of Medicine, University of Virginia, Charlottesville, Virginia, USA

[13]Department of Neuroradiology,University of Texas MD Anderson, Houston, TX 77030-4009

Abstract

An orthotopically allografted mouse GL26 glioma model ($Ccr2^{RFP/wt}$-$Cx3cr1^{GFP/wt}$) was used to evaluate the effect of transient, focal opening of the Blood Brain Barrier (BBB) on the composition of tumor-associated macrophages and microglia (TAMs). BBB Opening was induced by Magnetic Resonance Imaging (MRI)-guided focused ultrasound (MRgFUS) combined with microbubbles. CX3CR1-GFP cells and CCR2-RFP cells in brain tumors were quantified in microscopic images. Tumors in animals treated with a single session of MRgFUS did not show significant changes in cell numbers when compared to tumors in animals not receiving FUS. However, tumors that received two or three sessions of MRgFUS showed significantly increased amounts of both CX3CR1-GFP and CCR2-RFP cells.

The effect of MRgFUS on immune cell composition was also characterized and quantified utilizing flow cytometry. Glioma implantation resulted in increased amounts of lymphocytes, monocytes, and neutrophils in the brain parenchyma. Tumors administered MRgFUS showed increased numbers of monocytes and monocyte-derived TAMs. In addition, MRgFUS-treated tumors exhibited more CD80+ cells in monocytes and microglia.

In summary, transient, focal opening of the BBB using MRgFUS combined with microbubbles can activate the homing and differentiation of monocytes, and induce a shift towards a more proinflammatory status of the immune environment in glioblastoma.

Keywords

Sterile inflammation; Glioblastoma; TAMs; microglia and macrophage activation; Focused Ultrasound; MRgFUS; microbubbles

INTRODUCTION

Glioblastoma (GBM) is the most common and most lethal primary malignancy of the central nervous system. With an incidence of 2–3 per 100,000 population, GBM makes up to 54% of all gliomas and 16% of all primary brain tumors (Ostrom, et al. 2020). Even with multimodal treatments including surgery, chemotherapy and radiotherapy, the median survival time for patients with GBM is only 14.6 months (Thakkar, et al. 2014, Louis, et al. 2021). Despite recent advances in the development of novel therapies against extracranial tumors, very little progress has been made in terms of patient outcome for the treatment of GBM (Maxwell, et al. 2017). The lack of progress in the development of novel therapies for brain tumors can be attributed, at least in part, to the difficulty of therapeutic agents to

cross the blood-brain barrier (BBB) and the dose limited-toxicity that restricts the injection of therapeutic dosages.

The BBB regulates access to the the central nervous system through a tightly regulated neurovascular unit (NVU) including endothelial cells (ECs), pericytes and astrocytic endfeet, which together control the passage of nutrients and metabolites from the blood stream to the brain parenchyma. However, these same features also hinder the delivery of systemic therapies into brain tumors. While the BBB is often disturbed in brain tumor tissue, the disruption is heterogeneous and only allows smaller molecules to enter, resulting in inadequate drug accumulation in glioblastomas (Sarkaria, et al. 2018) (Zhou, et al. 2017). Consequently, the structural and functional heterogeneity of the BBB in the brain tumor microenvironment needs to be considered when attempting to develop effective, systemically-delivered therapies. Multiple strategies are being developed to regulate or disrupt BBB, including the use of osmotic agents (Gumerlock, et al. 1992, Rodriguez, et al. 2015, Duskey, et al. 2017) and the design of molecules utilizing receptor-mediated transport (Lajoie and Shusta 2015).

Transcranial magnetic resonance imaging (MRI)-guided focused ultrasound (MRgFUS), combined with intraveneous microbubbles, has also emerged as an effective strategy for non-invasively opening the BBB (Jolesz and Mcdannold 2014). MRgFUS oscillates microbubbles and mechanically disrupts the BBB in a targeted, transient, and non-invasive manner, increasing the vascular permeability to large molecules into the brain (Fry, et al. 1958, Fry 1958, Hynynen, et al. 2003). In preclinical studies, MRgFUS-induced opening of the BBB has been used to deliver chemotherapeutic agents (Treat, et al. 2012, Mainprize, et al. 2019), antibodies (Kinoshita, et al. 2006, Jordao, et al. 2010), stem cells (Burgess, et al. 2011), and therapeutic genes (Noroozian, et al. 2019). Extensive preclinical research has shown that FUS with microbubbles can lead to a more than 4-fold increase in the delivery and penetration of a range of intravenously administered anticancer agents in brain tumors (Aryal, et al. 2014). This improvement in the delivery of anticancer agents has also led to a significant increase in the median survival time (3-fold) in multiple orthotopic murine tumor models, including glioma and breast cancer brain metastasis (Arvanitis, et al. 2018).

Most of the research on MRgFUS-induced BBB opening has focused on using this approach to increase the concentration of therapeutic agents in brain tumors. However, MRgFUS by itself may also directly induce some immune-related responses. Studies on naïve animals have shown that MRgFUS-induced BBB opening elicited sterile inflammation in the normal brain microenvironment. MRgFUS-induced opening of the BBB triggers an acute increase in the transcription of proinflammatory cytokines (Kovacs, et al. 2017, Mcmahon, et al. 2017). In intracranial tumor models, MRgFUS combined with microbubbles also has immunomodulatory effects (Chen, et al. 2015). MRgFUS treated gliomas exhibit an increase in the CD8+/T-reg ratio, a metric commonly correlated with improved treatment outcome (Chen, et al. 2015). The immunomodulatory influence of MRgFUS combined with microbubbles on the BBB may thus provide an opportunity for synergy of MRgFUS and immune based therapeutics that could generate a stronger clinical response. A key step in evaluating this intriguing possibility is to investigate how MRgFUS affects the tumor-associated macrophages and microglia (TAMs) in the GBM-TAM pool.

In the current study, we applied MRgFUS together with microbubbles to an immunocompetent mouse glioma model based on orthotopic implantation of GL26 glioma cells. To investigate the composition and functional status of myeloid populations after BBB opening, tumor cells were allografted to $Ccr2^{RFP/wt}Cx3cr1^{GFP/wt}$ mice carrying genetically color-coded microglia (Cx3cr1-GFP) and blood-derived monocytes and macrophages (Ccr2-RFP). Multistain immunochemistry and flow cytometry (FCM) were utilized to define the changes of TAMs after MRgFUS treatment.

MATERIALS and METHODS

Study design

The animal protocol for this study was approved by the Stanford University Administrative Panel on Laboratory Animal Care (APLAC). All experiments were conducted in accordance with the National Institutes of Health's Guide for the Care and Use of Laboratory Animals. Two series of experiments were carried out, one for histological analysis and one for FCM analysis.

Thirty mice with brain tumors were divided into six groups that received the following treatments prior to histology analysis:

- Group 1: No MRgFUS – control group – animals were euthanized when the tumors were 4–5 mm in diameter (n=5).
- Group 2: MRgFUSx1 – one session of MRgFUS when the tumors were 4mm in diameter and the animals were euthanized 2 days after MRgFUS (n=5).
- Group 3: MRgFUSx2 – two sessions of MRgFUS every other day starting when the tumors were 3–4 mm in diameter and euthanized at 2 days after the second session of MRgFUS (n=5).
- Group 4: MRgFUSx3 – three sessions of MRgFUS, once every other day, starting when the tumors were a 2–3mm in diameter, euthanized at 2 days after the last session of MRgFUS (n=5).

The other ten animals were divided into 2 groups that received the following treatments prior to FCM analysis.

- Group 5: Tumor_No FUS, animals were euthanized when the tumors were 4–5 mm in diameter (n=5).
- Group 6: Tumor_FUS, three sessions of MRgFUS, once every other day, starting when the tumors were a 2–3mm in diameter, euthanized at 2 days after the last session of MRgFUS (n=5).

Three naïve animals without brain tumors were euthanized to collect brain tissue for FCM analysis.

Cell Line and Culture

The GL26 mouse glioma cell line was provided by Dr. Ramasamy Paulmurugan and maintained in media consisting of DMEM, 10% FBS, 100ul/ml Penicillin-Streptomycin, and 4mM L-glutamine.

Mice

All mice were housed in specific pathogen-free conditions at a barrier facility at Canary Center at Stanford University School of Medicine (Stanford, California). All animal handling, surveillance, and experimentation was performed in accordance with and approval from the Stanford University Administrative Panel on Laboratory Animal Care.

Homozygous $Ccr2^{RFP/RFP}$ mice (JAX stock #017586) (Saederup, et al. 2010) and Cx3cr1-GFP mice (JAX stock #005582) (Jung, et al. 2000) on a C57BL/6 background were purchased from the Jackson Laboratory and intercrossed to yield $Ccr2^{RFP/wt}Cx3cr1^{GFP/wt}$ animals. To confirm the establishment of heterozygous mice, ear snips were collected when the offspring were 15 through 18 days old, and genotyping was performed using a commercial assay service (Transnetyx, Inc). Previous studies (Chen, et al. 2017) have shown that implantation of murine GL261 glioma cells to the $Ccr2^{RFP/wt}Cx3cr1^{GFP/wt}$ *dual knock-in* mice allowed for efficient evaluation of the myeloid cells, known to constitute the majority of CD45+ immune cells in gliomas. Immunohistochemistry allows for discrimination of CX3CR1-GFP+ microglia and TAMs derived thereof and CCR2-RFP+ blood-derived monocytes and monocyte-derived TAMs within the tumor as well as in surrounding adjacent brain.

Orthotopic syngeneic model of mouse brain tumors

Mouse glioma GL26 cells dissociated into single-cells suspensions were orthotopically injected into the brain of 8 to 10-week-old $Ccr2^{RFP/wt}Cx3cr1^{GFP/wt}$ mice using sterotactic injection. In brief, mice were anesthetized with 3% isoflurane (Minrad International, Buffalo, NY, USA) in an induction chamber. Anesthesia on the stereotactic frame (David Kopf Instruments, Tujunga, CA, USA) was maintained with 2% isoflurane/L oxygen delivered through a nose adaptor. A burr hole was placed 1.7 mm lateral and 2 mm posterior of bregma. A blunt-ended needle (75N, 26s/2”/2, 5 μL; Hamilton Co., Reno, NV, USA) was lowered into the burr hole to a depth of 3.5 mm below the dura surface and retracted 0.5 mm to form a small reservoir. Using a microinjection pump (UMP-3; World precision Instruments, Sarasota, FL, USA), 4×10^5 GL26 cells were injected in a volume of 3 μL at 30 nL/s. After leaving the needle in place for 1 minute, it was retracted at 3 mm/min. The cranial injection site was sealed using biodegradable glue. Tumor formation was followed by MRI using a 3-tesla scanner from MR Solutions. From 1-week post tumor implantation, T2- Fast spin echo (FSE, repetition time/echo time [TR/TE] =4800/68 ms, flip angle 90°, 2 averages, field of view 28 mm, matrix size=256×248, slice thickness 1.0 mm) images were acquired once every 2 days to monitor the growth of the tumor. T2*-weighted gradient echo images (repetition time/echo time [TR/TE]=391/13 ms, flip angle 20°, 3 averages, field of view 28 mm, matrix size=256×256, slice thickness 1.0 mm) were obtained in order to identify possible hemorrhage.

MRgFUS set up and treatment protocol

MRgFUS was delivered to open the BBB. The MRgFUS system (Image Guided Therapy, Pessac, France) was configured as described in previous studies (Zhang, et al. 2015, Zhang, et al. 2016). The system included an MR-compatible, pre-focused, eight-element annular array, 1.5-MHz transducer (spherical radius = 20+/−2 mm, active diameter=25 mm [focal ratio =0.8]; Imasonic, Voray sur l'Ognon, France), which was connected to a phased array generator and radiofrequency power amplifier. The transducer and animals were prepared as described in a previous study (Zhang, et al. 2020). The membrane in front of the transducer was filled with degassed water and acoustic gel was applied between the transducer and skin. For sonication, the animals were placed in a prone position and maintained in that position using a bite bar and ear bars. The scalp hair was shaved and removed with depilatory cream. The experimental apparatus in this study is shown in Figure 1.

Definity® Microbubbles (mean diameter range: 1.1–3.3 μm, mean concentration of 1.2×10^{10} bubbles per mL, diluted by 1:20 using 1×PBS, 300 μL/kg, Lantheus Medical Imaging, MA, USA) were injected through a catheter placed in tail vein just before sonication (1.5 MHz, pulse duration 20-ms, duty cycle of 2%, 1-Hz pulse repetition frequency, 90-s duration per sonication). Multiple sonications were administered in the vicinity of the targeted area of the brain by moving the sonication zones slightly rostro-caudally and medio-laterally targeting the brain tumors. An MR-compatible motorized positioning stage was used to move the transducer in the rostral-caudal and medial-lateral directions. After determining the coordinates of the focal point within the MRI space, treatment planning MRI was acquired, and the focal region was positioned within the tumor. Ultrasound bursts were then applied at peak negative pressure of 0.5MPa.

MRI Data Collection

On the day prior to, and immediately post MRgFUS, a set of MRI data including T2-FSE, T2*-weighted gradient echo, dynamic contrast-enhanced (DCE), and post-contrast T1-weighted images was obtained.

The pre and post-MRgFUS T2-FSE images were acquired in order to assess the size and location of the resulting lesions, T2*-weighted gradient echo images were obtained to identify possible hemorrhagic complications from the MRgFUS procedure. In order to obtain quantitative measurements of BBB permeability, a bolus of gadodiamide contrast (gadobenate dimeglumine; Multihance, Bracco Diagnostics Inc., Monroe Township, NJ 08831, USA) was injected intravenously for DCE imaging (TR/TE = 34/3 ms, average = 1, FOV 28 mm^2, flip angle 20°). Post-contrast T1-weighted imaging (TR/ TE =620/12 milliseconds, 2 averages, field of view=28 mm, matrix size=256×244, slice thickness=1 mm) was utilized to confirm the opening of the BBB after DCE imaging. Images were reviewed and analyzed using the Horos DICOM viewer. Using FDA-approved commercial software NordicICE (Nordic Neuro Lab, Bergen, Norway), Ktrans maps were computed by using a pipeline inspired by that of Anzalone et al (Anzalone, et al. 2018). Notably, local AIF adapted for mice studies were extracted from the signal curves using a blind deconvolution method (Jirik, et al. 2019).

Tissue Preparation and Analysis

Mice were euthanized with inhalation of 3% isoflurane 2 days after the last MRgFUS session and perfused through the left ventricle at 15 mL/min for 1 min with 0.9% NaCl and then for 30 min with 4% paraformaldehyde in 0.1 M phosphate buffer solution (PBS, pH 7.4). Brains tissues were post-fixed overnight at 4°C and then transferred into 30% (w/v) sucrose in PBS. After equilibrating in the 30% sucrose solution, the brains were sectioned coronally (30 μm) with a sliding microtome. Sections were collected in 30% ethylene glycol and 25% glycerol in 50 mM PBS and stored at −20°C until used. A 1-in-6 series of sections were collected for nuclear counterstaining with Invitrogen Hoechst 33342 dye. Coronal brain sections containing tumors were acquired with a NanoZoomer Digital Pathology slide scanning system (Hamamatsu Photonics, K.K., Japan).

In order to analyze the histological images, a custom analysis pipeline was setup in order to provide a tool able to quantify in a semi-automated manner the number of GFP and RFP labeled cells per mm^2 on the brain sections. On the images of the stained sections of the brain through Nanozoomer, a Region of Interest (ROI) was drawn around the brain tumor with the Freehand drawing tool of NDP.view2 software (Hamamatsu Photonics, K.K., Japan) by the the investigators blinded to the identity of the animals and sections they were analyzing. In order to minimize the bias in quantifying the GFP-labeled cells and the RFP-labeled cells, the red and green channel were set both at full dynamic ranges of 200% while the dynamic range of blue channel was switched to 0% and turned off. A simple filter was used to improve the resolution of the image and a magnification factor of 1.8 to 2.5% was applied to the ROIs. Then, the images were exported in .jpg files and analyzed in FIJI (ImageJ). FIJI is an open source software commonly used for biomedical image analysis (Schindelin, et al. 2012). Upon loading the images in FIJI, the background was first removed using the Rolling Ball Radius algorithm (Kuwahara and Eiho 1983, Sternberg R. 1983). The red and the green channels were then split, and considering the different sizes of the RFP-labeled cells and the GFP-labeled cells, two different radii were adopted to subtract the red and the green components from the background. Otsu thresholding was used on the red and green channel images separately to distinguish positive from negative signals (Hetal J. Vala 2013, Hetal J. Vala 2013). The group above the threshold (automatically computed based on signal intensity in the gray scale) was recognized as the effective signal from the labeled cells and the group below the threshold was recognized as background noise and discarded. The application of a binary mask was followed by the watershed separation as a robust segmentation method, based on the average size of recognized single cells (Ankit Chadha 2013). Finally, a simple particle counting method was applied to the resulting images (for the green channel and the red channel) taking into account the average size of the single cells in order to quantify the number of GFP and RFP cells per mm^2. T-test was used to compare the number of GFP and RFP cells per mm^2 from two different groups.

FCM analysis

Mice were deeply anesthetized with 1–4% isofluorane through a nosecone, and transcardially perfused with ice-cold PBS. Brain specimens (left and right brain parenchyma from naïve animals; left and right brain parenchyma, and tumor tissue from the animals with gliomas) were dissected and dissociated into single-cell suspensions using the Brain Tumor

Dissociation Kit (Miltenyi Biotech, Catalog # 130-095-942). Cells were then resuspended in ice-cold FCM buffer containing HBSS without Calcium and Magnesium, 2% FBS, and 10mM HEPES. Zombie Nir (Biolegend) staining was applied to exclude dead cells (20 min at 4 °C degree), followed by a rinse using an ice-cold FCM buffer. Commercially available rat-anti-mouse CD16/32 antibody (Biolegend) staining for Fc-blocking (20 min at 4 °C degree) followed by washing in ice-cold FCM buffer were employed to eliminate nonspecific binding. The cells were then stained with fluorochroma-conjugated antibodies for 30 min at 4 °C degree in dark (Table 1), followed by washing in ice-cold FCM buffer. All data were collected on a BD LSR flow cytometer and analyzed using FlowJo 10 software v10.6.1 (Tree Star Inc.).

Lymphocytes and myeloid cells were identified from viable cells through cell membrane markers CD45 and CD11b. Microglia, monocytes, and neutrophils were identified from myeloid cells through the expression of CX3CR1-GFP and CCR2-RFP. F4/80 was used to differentiate the monocyte-derived tumor associated macrophages (Mo-TAMs) from Naïve monocytes (Mo); and the microglia-derived tumor associated macrophages (Mg-TAMs) from Naïve microglia (Mg). CD80 and CD206 were applied to discriminate the CD80+ pro-inflammatory and CD206+ anti-inflammatory of microglia and monocytes. (Supplementary figure.1).

Statistical analysis

Mean±SD was used for continuous variables with normal distribution. One-way analysis of variance (ANOVA) followed by Dunnett's post hoc test was conducted to compare the cell density of CX3CR1-GFP, CCR2-RFP cells between each individual treatment group of FUSx1, FUSx2, or FUSx3 and Tumor_NO FUS group from histological analysis. One-way analysis of variance (ANOVA) followed by post hoc Bonferroni correction was obtained for multigroup comparisons of the cells identified with fluorochrome-conjugated antibodies in FCM analysis. Probability values of less than 0.05 were considered statistically significant. The statistical software IBM SPSS version 22 was used for the statistical analyses.

RESULTS

Confirmation of BBB Opening

On baseline imaging pre-MRgFUS, all 30 tumors showed enhancement, with heterogenous enhancement in 24 tumors and homogenous enhancement in 6 tumors. All of the animals treated with MRgFUS showed enhancement on the postcontrast T1-weighted images in the brain parenchyma along the sonicated area, both in the tumor (more pronounced enhancement than at baseline) and outside the tumor, demonstrating the successful opening of the BBB by MRgFUS. Immediately after sonication, there was no edema on T2-weighted images and no evidence of hemorrhage induced by MRgFUS on T2*-weighted gradient echo images. The post-FUS Ktrans values increased significantly compared to the pre-FUS_FUS ones ($P=0.03$, Figure 2B).

MRgFUS increases infiltration of CX3CR1-GFP and CCR2-RFP cells into the tumor area

GL26 glioma tissues were diffusely infiltrated with CX3CR1-GFP and CCR2-RFP cells in all animals receiving tumors. In the group receiving tumor cell implantation but no FUS (Tumor_No FUS), single-positive CX3CR1-GFP (Figure 3A, first row, arrows) and CCR2-RFP (Figure 3A, first row, arrowheads) cells were scattered in the core region of the tumor, and the fluorescent cells were mainly dual-positive cells (Figure 3A, first row, triangles). There were more CX3CR1-GFP and CCR2-RFP dual-positive cells (Figure 3A, second row, triangles) at the tumor egde. Single-positive CX3CR1-GFP (Figure 3A, third row, arrows), CCR2-RFP (Figure 3A, third row, arrowheads), and dual-positive cells were seen in the peritumoral area, with single-positive CX3CR1-GFP cells seen more frequently seen than CCR2-RFP cells. In the animals that received 3 sessions of MRgFUS (Figure 3B), there was an substantial increase in CCR2-RFP and CX3CR1-GFP cells. The quantification analysis showed a significant increase in the number of green cells and red cells in the animals treated with 2 and 3 sessions of MRgFUS (Figure 3C).

Immune micro-enviroment of naïve brain and the brain tissue implanted with GL26 glioma

Microglia (CX3CR1+CCR2−) is the predominant parenchymal immune cell in the naïve brain, the ipsilateral parenchyma, and the contralateral parenchyma in the brain allografted with GL26 tumor. Compared to the naïve brain, the ipsilateral parenchyma of the brains allografted with tumor showed more lymphocytes (p=0.001), monocytes(p=0.001), and neutrophils (p=0.04), and relatively lower proportion of microglia (p=0.001). The contralateral parenchyma displayed the same changes (lymphocytes: p=0.001, monocytes: p=0.002, neutrophils: P=0.02, microglia: p=0.002). The proportions of the immune cells between the ipsilateral and contralateral parenchyma did not show significant difference. Compared with naïve brain, the allografted parenchyma showed more monocyte-derived TAMs (ipsilateral parenchyma: p=0.003, contralateral parenchyma: p=0.03), and more microglia-derived TAMs (ipsilateral parenchyma: p=0.005, contralateral parenchyma: p=0.02). The bilateral parenchyma of the brain allografted with tumor did not show significant difference in the differentiation of the monocytes (p=0.88) and microglia (p=0.44).

There were more proinflammation CD80+ cells in monocytes (ipsilateral parenchyma: p=0.01, contralateral parenchyma: p=0.04) and microglia (ipsilateral parenchyma: p=0.04, contralateral parenchyma: p=0.002) of the ipsilateral and contralateral parenchyma compared with the naïve brain. The proportion of CD206+ cells in the contralateral parenchyma (p=0.03) was lower than the one from naïve brain. (Figure 4)

Effects of MRgFUS on the immune micro-enviroment of tumor tissue

The animals treated with MRgFUS showed increased monocytes ($p=0.01$) and decreased proportion of neutrophils ($p=0.03$) compared to the Tumor_No FUS group. The proportions of lymphcytes (p=0.69), myeloid cells (p=0.67), and microglia (p=0.76) did not show any significant difference between the gliomas from the Tumor_No FUS and Tumor_FUS groups (Figure 5D and 5E). Tumor_FUS group showed more monocytes differentiation: higher proportion of monocytes-derived TAMs (p=0.04), whereas microglia did not show changes in differentiation (p=0.19) (Figure 5F). In the tumors treated with FUS,

there were more proinflammation CD80+ cells both in CCR2+ monocytes(p=0.03) and CX3CR1+CCR2− microglia cells (p=0.05). (Figure 5G, 5H).

DISCUSSION

As the most common and aggressive primary brain tumor, GBMs display a high degree of inter- and intra-tumor heterogeneity. The most prevalent non-neoplastic cell population in the GBM microenvironment is comprised of cells of the innate immune system called TAMs, which represent approximately 30–40% of the cells in a GBM (Charles, et al. 2012). These cells have been shown to engage in reciprocal interactions with neoplastic tumor cells to either inhibit or promote tumor growth and progression (Feng, et al. 2015, Hu, et al. 2015). Efforts have been made to achieve a “re-education” of TAMs by polarizing them toward an M1-like proinflamatory signature from an M2-like anti-inflamatory/tumorigenic signature, with the goal of creating a less supportive tumor microenvironment (Wang, et al. 2017, Chen and Hambardzumyan 2018). The purpose of the present study was to evaluate the possibility that treatment with MRgFUS can modify the immune status of the tumor microenvironment in a model of GBM.

As a noninvasive technique that can induce transient BBB opening in targeted brain regions, MRgFUS combined with microbubbles has been shown to successfully deliver large molecules into the brain parenchyma without evidence of micro-hemorrhages (Hynynen, et al. 2001, Tung, et al. 2010). This approach has been used to facilitate the delivery of drugs and genes to treat stroke, neurodegenerative disease, and primary and metastatic brain tumors in animal models (Burgess, et al. 2014, Burgess and Hynynen 2014, Kovacs, et al. 2014, Leinenga, et al. 2016). Promising findings from extensive animal research led to clinical trials in patients with Glioblastoma (GBM) (NCT02253212, NCT04118764) and Alzheimer’s disease (AD) (NCT04118764). Initial feasibility and safety were established in patients with GBM (Idbaih, et al. 2019) and AD (Lipsman, et al. 2018), with corresponding trials showing safe and reversible BBB opening using a clinical MR-guided focused ultrasound system.

In addition, MRgFUS by itself may directly exert certain immune-related effects. In studies of normal brain, MRgFUS combined with microbubbles induces microglia activation (Alonso, et al. 2011, Kovacs, et al. 2017, Sinharay, et al. 2019), and elicits macrophage homing from the periphery to sonicated regions of the brain (Kovacs, et al. 2017). Studies using mouse models of Alzheimer’s disease have shown that repeated MRgFUS treatments lead to a 20% reduction in Amyloid-β plaque load (Jordao, et al. 2013, Burgess, et al. 2014), effects that may be the result of MRgFUS-induced increases in endogenous immunoglobulins, activated microglia, and activated astrocytes. Although sterile inflammation, microglial activation, and macrophage homing produced by MRgFUS have been well studied, there is little known about how MRgFUS impacts the cellular phenotypes of TAMs.

In our study, histological assessments did not demonstrate significant changes in the CX3CR1− GFP or CCR2-RFP cells in tumors that received only one session of MRgFUS. However, tumors that received two or three sessions of MRgFUS showed increased numbers

of CX3CR1-GFP cells and CCR2-RFP cells, with the animals receiving three sessions exhibiting the most abundant increases. One limitation of using histological quantification of cellular phenotypes is the difficulty in defining the number of dual-positive cells, which form the predominant population of TAMs. Consequently, in order to distinguish among the CX3CR1-GFP, CCR2-RFP, and CX3CR1-GFP/CCR2-RFP dual positive cells in the TAMs pool, FCM was used to analyze the immune cells in naïve brain parenchyma, brain parenchyma ipsilateral and contralateral to a tumor, and in brain tumors that did or did not receive MRgFUS treatment. In naïve brains, almost all of the myeloid cells were CX3CR1+CCR2− microglia. Implantation of GL26 glioma cells into the brain significantly modified the immune environment of the brain parenchyma. In both the ipsilateral and contralateral parenchyma of the brain implante with GL26 glioma, the proportions of lymphocytes, monocytes, neutrophils, and the differentiated cells, including monocytes-derived TAMs and microglia-derived TAMs were increased significantly, while the proportion of microglia was decreased. Both monocytes and microglia showed more proinflammation CD80+ cells.

FCM findings demonstrated an increase in monocytes in tumors treated with MRgFUS, which is consistent with findings from previous studies showing that MRgFUS causes macrophages to home to a sonicated region (Kovacs, et al. 2017). The tumors treated with MRgFUS showed more differentiated TAMS from monocytes. These findings indicate that MRgFUS induces homing of monocytes and promotes differentiation of TAMs. Previous studies investigeted sterile inflammation from the BBB opening induced by MRgFUS in different species of labotory animals (Kovacs, et al. 2017, Mcmahon, et al. 2017), with various microbubble fomulations or doses. Kovacs and the coauthors infused 100 μL Optison into 8- to 10-wk-old Sprague-Dawley rats and sonicated with a single-element spherical FUS transducer with center frequency at 589.636 KHz. Mcmahon and coauthors administered Definity at 20 μL /kg to Sprague-Dawley rats weighing 200–300 g, and sonicated with a transducer at a frequency of 551.5 kHz. In this study, transducer at 1.5 MHz was applied to sonicate mouse brain with glioma, with Definity microbubbles diluted by 1:20 at 300 μL/kg body weight, which has been proved successfully opening mouse BBB in our previous studies.

Under physiological conditions, immune cells in naïve brains do not show pro-inflammatory or anti-inflammatory phenotypes, based on the lack of CD80+ or CD206+ cells. The animals from the Tumor_FUS group showed more CD80+ cells in both monocytes and microglia, while the number of CD206+ was changed. This indicates that MRgFUS induces monocytes and microglia in the direction of pro-inflammatory polarization. This may be the result of the increased expression of cytokines after MRgFUS. Previous evidence of MRgFUS-induced sterile inflammation in normal brain (Kovacs, et al. 2017) has shown an immediate increase in multiple cytokines including TNFα, IL1α, IL1β, and IL18. These changes could in turn induce an increase in chemotactic factors for immune cells (MCP1, G-CSF, GM-CSF, MIP3α, and RANTES), among which IL1β and TNFα are pro-inflammatory cytokines.

CONCLUSIONS

Treatment of tumors with MRgFUS combined with microbubbles promotes the homing and differentiation of monocytes and induces the polarization of monocytes and microglia in a pro-inflammatory direction. This non-invasive procedure therefore holds promise for future development both as a stand-alone therapeutic strategy, as well an adjunct strategy for facilitating the delivery of chemotheraputic agents for the treatment of GBM.

Supplementary Material

Refer to Web version on PubMed Central for supplementary material.

Acknowledgments

This work was supported by National Institutes of Health Grants R01 CA217953-01 and R01 NS102194.

Abbreviations

BBB	Blood Brain Barrier
TAMs	Tumor-associated macrophages and microglia
MRI	Magnetic Resonance Imaging
MRgFUS	Magnetic Resonance Imaging-guided focused ultrasound
CX3CR1	CX3C chemokine receptor 1
CCR2	C-C chemokine receptor type 2
GFP	Green fluorescent protein
RFP	Red fluorescent protein
WT	Wild type
CD45	Protein tyrosine phosphatase receptor type C (PTPRC)
CD11b	Integrin alpha M (ITGAM)
F4/80	EGF-like module-containing mucin-like hormone receptor-like 1 (EMR1)
Ly6C	Lymphocyte antigen 6C
Ly6G	Lymphocyte antigen 6 complex locus G6D
CD80	Cluster of differentiation 80
CD206	Cluster of Differentiation 206
GBM	Glioblastoma
NVU	neurovascular unit

ECs	Endothelial cells
FCM	Flow cytometry
APLAC	Administrative Panel on Laboratory Animal Care
TR/TE	Repetition time/echo time
FSE	Fast spin echo
DCE	Dynamic contrast-enhanced
GRE	Gradient echo image
PBS	Phosphate buffer solution
ROI	Region of Interest
TNFα	Tumor necrosis factor alpha
IL1α	Interleukin 1 alpha
IL1β	Interleukin 1 beta
IL18	Interleukin-18
MCP1	Monocyte chemoattractant protein-1
G-CSF	Granulocyte colony stimulating factor
GM-CSF	Granulocyte macrophage-colony stimulating factor
MIP3α	Macrophage Inflammatory Protein-3α
RANTES	Regulated upon Activation, Normal T Cell Expressed and Presumably Secreted

REFERENCES

Alonso A, Reinz E, Fatar M, Hennerici MG, Meairs S. Clearance of albumin following ultrasound-induced blood-brain barrier opening is mediated by glial but not neuronal cells. Brain Res 2011;1411:9–16. [PubMed: 21820103]

Ankit Chadha NS. A Robust Approach to Image Segmentation with Optimal Thresholding and Watershed Transform. International Journal of Computer Applications 2013;65:1–7.

Anzalone N, Castellano A, Cadioli M, Conte GM, Cuccarini V, Bizzi A, Grimaldi M, Costa A, Grillea G, Vitali P, Aquino D, Terreni MR, Torri V, Erickson BJ, Caulo M. Brain Gliomas: Multicenter Standardized Assessment of Dynamic Contrast-enhanced and Dynamic Susceptibility Contrast MR Images. Radiology 2018;287:933–43. [PubMed: 29361245]

Arvanitis CD, Askoxylakis V, Guo Y, Datta M, Kloepper J, Ferraro GB, Bernabeu MO, Fukumura D, McDannold N, Jain RK. Mechanisms of enhanced drug delivery in brain metastases with focused ultrasound-induced blood-tumor barrier disruption. Proc Natl Acad Sci U S A 2018;115:E8717–E26. [PubMed: 30150398]

Aryal M, Arvanitis CD, Alexander PM, McDannold N. Ultrasound-mediated blood-brain barrier disruption for targeted drug delivery in the central nervous system. Adv Drug Deliv Rev 2014;72:94–109. [PubMed: 24462453]

Burgess A, Ayala-Grosso CA, Ganguly M, Jordao JF, Aubert I, Hynynen K. Targeted delivery of neural stem cells to the brain using MRI-guided focused ultrasound to disrupt the blood-brain barrier. PLoS One 2011;6:e27877. [PubMed: 22114718]

Burgess A, Dubey S, Yeung S, Hough O, Eterman N, Aubert I, Hynynen K. Alzheimer disease in a mouse model: MR imaging-guided focused ultrasound targeted to the hippocampus opens the blood-brain barrier and improves pathologic abnormalities and behavior. Radiology 2014;273:736–45. [PubMed: 25222068]

Burgess A, Hynynen K. Drug delivery across the blood-brain barrier using focused ultrasound. Expert Opin Drug Deliv 2014;11:711–21. [PubMed: 24650132]

Charles NA, Holland EC, Gilbertson R, Glass R, Kettenmann H. The brain tumor microenvironment. Glia 2012;60:502–14. [PubMed: 22379614]

Chen H, Hou GY, Han Y, Payen T, Palermo CF, Olive KP, Konofagou EE. Harmonic motion imaging for abdominal tumor detection and high-intensity focused ultrasound ablation monitoring: an in vivo feasibility study in a transgenic mouse model of pancreatic cancer. IEEE Trans Ultrason Ferroelectr Freq Control 2015;62:1662–73. [PubMed: 26415128]

Chen PY, Hsieh HY, Huang CY, Lin CY, Wei KC, Liu HL. Focused ultrasound-induced blood-brain barrier opening to enhance interleukin-12 delivery for brain tumor immunotherapy: a preclinical feasibility study. J Transl Med 2015;13:93. [PubMed: 25784614]

Chen Z, Feng X, Herting CJ, Garcia VA, Nie K, Pong WW, Rasmussen R, Dwivedi B, Seby S, Wolf SA, Gutmann DH, Hambardzumyan D. Cellular and Molecular Identity of Tumor-Associated Macrophages in Glioblastoma. Cancer Res 2017;77:2266–78. [PubMed: 28235764]

Chen Z, Hambardzumyan D. Immune Microenvironment in Glioblastoma Subtypes. Front Immunol 2018;9:1004. [PubMed: 29867979]

Duskey JT, Belletti D, Pederzoli F, Vandelli MA, Forni F, Ruozi B, Tosi G. Current Strategies for the Delivery of Therapeutic Proteins and Enzymes to Treat Brain Disorders. Int Rev Neurobiol 2017;137:1–28. [PubMed: 29132540]

Feng X, Szulzewsky F, Yerevanian A, Chen Z, Heinzmann D, Rasmussen RD, Alvarez-Garcia V, Kim Y, Wang B, Tamagno I, Zhou H, Li X, Kettenmann H, Ransohoff RM, Hambardzumyan D. Loss of CX3CR1 increases accumulation of inflammatory monocytes and promotes gliomagenesis. Oncotarget 2015;6:15077–94. [PubMed: 25987130]

Fry FJ, Ades HW, Fry WJ. Production of reversible changes in the central nervous system by ultrasound. Science 1958;127:83–4. [PubMed: 13495483]

Fry WJ. Intense ultrasound in investigations of the central nervous system. Adv Biol Med Phys 1958;6:281–348. [PubMed: 13825475]

Gumerlock MK, Belshe BD, Madsen R, Watts C. Osmotic blood-brain barrier disruption and chemotherapy in the treatment of high grade malignant glioma: patient series and literature review. J Neurooncol 1992;12:33–46. [PubMed: 1541977]

Hetal J Vala AB. A review on Otsu image segmentation algorithm.. International Journal of Advanced Research in Computer Engineering and Technology 2013;2:387–89.

Hetal J Vala AB. A review on Otsu image segmentation algorithm.. International Journal of Advanced Research in Computer Engineering and Technology 2013;2:387–89.

Hu F, Dzaye O, Hahn A, Yu Y, Scavetta RJ, Dittmar G, Kaczmarek AK, Dunning KR, Ricciardelli C, Rinnenthal JL, Heppner FL, Lehnardt S, Synowitz M, Wolf SA, Kettenmann H. Glioma-derived versican promotes tumor expansion via glioma-associated microglial/macrophages Toll-like receptor 2 signaling. Neuro Oncol 2015;17:200–10. [PubMed: 25452390]

Hynynen K, McDannold N, Vykhodtseva N, Jolesz FA. Noninvasive MR imaging-guided focal opening of the blood-brain barrier in rabbits. Radiology 2001;220:640–6. [PubMed: 11526261]

Hynynen K, McDannold N, Vykhodtseva N, Jolesz FA. Non-invasive opening of BBB by focused ultrasound. Acta Neurochir Suppl 2003;86:555–8. [PubMed: 14753505]

Idbaih A, Canney M, Belin L, Desseaux C, Vignot A, Bouchoux G, Asquier N, Law-Ye B, Leclercq D, Bissery A, De Rycke Y, Trosch C, Capelle L, Sanson M, Hoang-Xuan K, Dehais C, Houillier C, Laigle-Donadey F, Mathon B, Andre A, Lafon C, Chapelon JY, Delattre JY, Carpentier A. Safety and Feasibility of Repeated and Transient Blood-Brain Barrier Disruption by Pulsed Ultrasound in Patients with Recurrent Glioblastoma. Clin Cancer Res 2019;25:3793–801. [PubMed: 30890548]

Jirik R, Taxt T, Macicek O, Bartos M, Kratochvila J, Soucek K, Drazanova E, Kratka L, Hampl A, Starcuk Z Jr. Blind deconvolution estimation of an arterial input function for small animal DCE-MRI. Magn Reson Imaging 2019;62:46–56. [PubMed: 31150814]

Jolesz FA, McDannold NJ. Magnetic resonance-guided focused ultrasound: a new technology for clinical neurosciences. Neurol Clin 2014;32:253–69. [PubMed: 24287394]

Jordao JF, Ayala-Grosso CA, Markham K, Huang Y, Chopra R, McLaurin J, Hynynen K, Aubert I. Antibodies targeted to the brain with image-guided focused ultrasound reduces amyloid-beta plaque load in the TgCRND8 mouse model of Alzheimer's disease. PLoS One 2010;5:e10549. [PubMed: 20485502]

Jordao JF, Thevenot E, Markham-Coultes K, Scarcelli T, Weng YQ, Xhima K, O'Reilly M, Huang Y, McLaurin J, Hynynen K, Aubert I. Amyloid-beta plaque reduction, endogenous antibody delivery and glial activation by brain-targeted, transcranial focused ultrasound. Exp Neurol 2013;248:16–29. [PubMed: 23707300]

Jung S, Aliberti J, Graemmel P, Sunshine MJ, Kreutzberg GW, Sher A, Littman DR. Analysis of fractalkine receptor CX(3)CR1 function by targeted deletion and green fluorescent protein reporter gene insertion. Mol Cell Biol 2000;20:4106–14. [PubMed: 10805752]

Kinoshita M, McDannold N, Jolesz FA, Hynynen K. Targeted delivery of antibodies through the blood-brain barrier by MRI-guided focused ultrasound. Biochem Biophys Res Commun 2006;340:1085–90. [PubMed: 16403441]

Kovacs Z, Werner B, Rassi A, Sass JO, Martin-Fiori E, Bernasconi M. Prolonged survival upon ultrasound-enhanced doxorubicin delivery in two syngenic glioblastoma mouse models. J Control Release 2014;187:74–82. [PubMed: 24878186]

Kovacs ZI, Kim S, Jikaria N, Qureshi F, Milo B, Lewis BK, Bresler M, Burks SR, Frank JA. Disrupting the blood-brain barrier by focused ultrasound induces sterile inflammation. Proc Natl Acad Sci U S A 2017;114:E75–E84. [PubMed: 27994152]

Kuwahara M, Eiho S. [Image processing technics--focus on software. 1. Perspectives in biomedical image processing]. Iyodenshi To Seitai Kogaku 1983;21:266–73. [PubMed: 6366293]

Lajoie JM, Shusta EV. Targeting receptor-mediated transport for delivery of biologics across the blood-brain barrier. Annu Rev Pharmacol Toxicol 2015;55:613–31. [PubMed: 25340933]

Leinenga G, Langton C, Nisbet R, Gotz J. Ultrasound treatment of neurological diseases--current and emerging applications. Nat Rev Neurol 2016;12:161–74. [PubMed: 26891768]

Lipsman N, Meng Y, Bethune AJ, Huang Y, Lam B, Masellis M, Herrmann N, Heyn C, Aubert I, Boutet A, Smith GS, Hynynen K, Black SE. Blood-brain barrier opening in Alzheimer's disease using MR-guided focused ultrasound. Nat Commun 2018;9:2336. [PubMed: 30046032]

Louis DN, Perry A, Wesseling P, Brat DJ, Cree IA, Figarella-Branger D, Hawkins C, Ng HK, Pfister SM, Reifenberger G, Soffietti R, von Deimling A, Ellison DW. The 2021 WHO Classification of Tumors of the Central Nervous System: a summary. Neuro Oncol 2021;23:1231–51. [PubMed: 34185076]

Mainprize T, Lipsman N, Huang Y, Meng Y, Bethune A, Ironside S, Heyn C, Alkins R, Trudeau M, Sahgal A, Perry J, Hynynen K. Blood-Brain Barrier Opening in Primary Brain Tumors with Non-invasive MR-Guided Focused Ultrasound: A Clinical Safety and Feasibility Study. Sci Rep 2019;9:321. [PubMed: 30674905]

Maxwell R, Jackson CM, Lim M. Clinical Trials Investigating Immune Checkpoint Blockade in Glioblastoma. Curr Treat Options Oncol 2017;18:51. [PubMed: 28785997]

McMahon D, Bendayan R, Hynynen K. Acute effects of focused ultrasound-induced increases in blood-brain barrier permeability on rat microvascular transcriptome. Sci Rep 2017;7:45657. [PubMed: 28374753]

Noroozian Z, Xhima K, Huang Y, Kaspar BK, Kugler S, Hynynen K, Aubert I. MRI-Guided Focused Ultrasound for Targeted Delivery of rAAV to the Brain. Methods Mol Biol 2019;1950:177–97. [PubMed: 30783974]

Ostrom QT, Patil N, Cioffi G, Waite K, Kruchko C, Barnholtz-Sloan JS. CBTRUS Statistical Report: Primary Brain and Other Central Nervous System Tumors Diagnosed in the United States in 2013–2017. Neuro Oncol 2020;22:iv1–iv96. [PubMed: 33123732]

Rodriguez A, Tatter SB, Debinski W. Neurosurgical Techniques for Disruption of the Blood-Brain Barrier for Glioblastoma Treatment. Pharmaceutics 2015;7:175–87. [PubMed: 26247958]

Saederup N, Cardona AE, Croft K, Mizutani M, Cotleur AC, Tsou CL, Ransohoff RM, Charo IF. Selective chemokine receptor usage by central nervous system myeloid cells in CCR2-red fluorescent protein knock-in mice. PLoS One 2010;5:e13693. [PubMed: 21060874]

Sarkaria JN, Hu LS, Parney IF, Pafundi DH, Brinkmann DH, Laack NN, Giannini C, Burns TC, Kizilbash SH, Laramy JK, Swanson KR, Kaufmann TJ, Brown PD, Agar NYR, Galanis E, Buckner JC, Elmquist WF. Is the blood-brain barrier really disrupted in all glioblastomas? A critical assessment of existing clinical data. Neuro Oncol 2018;20:184–91. [PubMed: 29016900]

Schindelin J, Arganda-Carreras I, Frise E, Kaynig V, Longair M, Pietzsch T, Preibisch S, Rueden C, Saalfeld S, Schmid B, Tinevez JY, White DJ, Hartenstein V, Eliceiri K, Tomancak P, Cardona A. Fiji: an open-source platform for biological-image analysis. Nat Methods 2012;9:676–82. [PubMed: 22743772]

Sinharay S, Tu TW, Kovacs ZI, Schreiber-Stainthorp W, Sundby M, Zhang X, Papadakis GZ, Reid WC, Frank JA, Hammoud DA. In vivo imaging of sterile microglial activation in rat brain after disrupting the blood-brain barrier with pulsed focused ultrasound: [18F]DPA-714 PET study. J Neuroinflammation 2019;16:155. [PubMed: 31345243]

Sternberg RS Biomedical Image Processing. IEEE Computer 1983;16:22–34.

Thakkar JP, Dolecek TA, Horbinski C, Ostrom QT, Lightner DD, Barnholtz-Sloan JS, Villano JL. Epidemiologic and molecular prognostic review of glioblastoma. Cancer Epidemiol Biomarkers Prev 2014;23:1985–96. [PubMed: 25053711]

Treat LH, McDannold N, Zhang Y, Vykhodtseva N, Hynynen K. Improved anti-tumor effect of liposomal doxorubicin after targeted blood-brain barrier disruption by MRI-guided focused ultrasound in rat glioma. Ultrasound Med Biol 2012;38:1716–25. [PubMed: 22818878]

Tung YS, Vlachos F, Choi JJ, Deffieux T, Selert K, Konofagou EE. In vivo transcranial cavitation threshold detection during ultrasound-induced blood-brain barrier opening in mice. Phys Med Biol 2010;55:6141–55. [PubMed: 20876972]

Wang Y, Lin YX, Qiao SL, An HW, Ma Y, Qiao ZY, Rajapaksha RP, Wang H. Polymeric nanoparticles promote macrophage reversal from M2 to M1 phenotypes in the tumor microenvironment. Biomaterials 2017;112:153–63. [PubMed: 27768970]

Zhang Y, Aubry JF, Zhang J, Wang Y, Roy J, Mata JF, Miller W, Dumont E, Xie M, Lee K, Zuo Z, Wintermark M. Defining the optimal age for focal lesioning in a rat model of transcranial HIFU. Ultrasound Med Biol 2015;41:449–55. [PubMed: 25542495]

Zhang Y, Tan H, Bertram EH, Aubry JF, Lopes MB, Roy J, Dumont E, Xie M, Zuo Z, Klibanov AL, Lee KS, Wintermark M. Non-Invasive, Focal Disconnection of Brain Circuitry Using Magnetic Resonance-Guided Low-Intensity Focused Ultrasound to Deliver a Neurotoxin. Ultrasound Med Biol 2016;42:2261–9. [PubMed: 27260243]

Zhang Y, Zhou H, Qu H, Liao C, Jiang H, Huang S, Ghobadi SN, Telichko A, Li N, Habte FG, Doyle T, Woznak JP, Bertram EH, Lee KS, Wintermark M. Effects of Non-invasive, Targeted, Neuronal Lesions on Seizures in a Mouse Model of Temporal Lobe Epilepsy. Ultrasound Med Biol 2020;46:1224–34. [PubMed: 32081583]

Zhou W, Chen C, Shi Y, Wu Q, Gimple RC, Fang X, Huang Z, Zhai K, Ke SQ, Ping YF, Feng H, Rich JN, Yu JS, Bao S, Bian XW. Targeting Glioma Stem Cell-Derived Pericytes Disrupts the Blood-Tumor Barrier and Improves Chemotherapeutic Efficacy. Cell Stem Cell 2017;21:591–603 e4. [PubMed: 29100012]

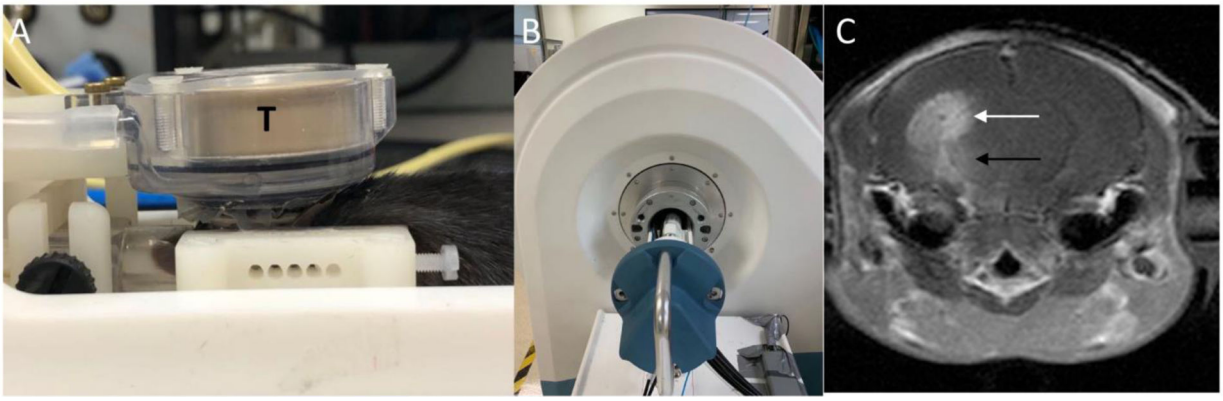

Figure 1. Experimental apparatus and post contrast T1-weighted image immediately after sonication.

A: MRgFUS system consisting of a 1.5-MHz transducer (T) that rests on the top of the mouse head and can move in X-Y planes and can be focused in the Z axis. B: A 3T MRI scanner was used to detect BBB-opening after sonication. C: Post-contrast T1-weighted image acquired immediately after sonication. Enhancement of the tumor (white arrow) and the brain tissue along the acoustic beam below the tumor (black arrow) indicates the area of BBB opening.

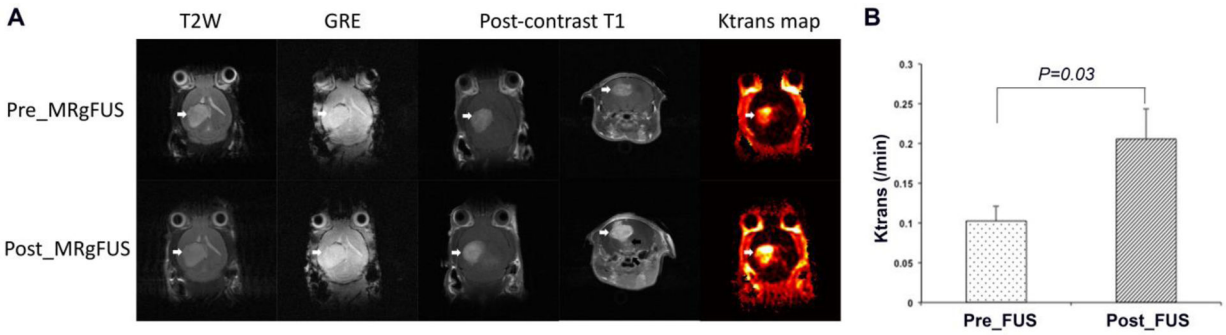

Figure 2. Examples of MR images of GL26 allograft acquired before and immediately post MRgFUS.

A) T2-weighted images did not show edema after MRgFUS. T2*-weighted gradient echo image (GRE) did not show hemorrhage from MRgFUS. Post-contrast T1-weighted images showed the enhancement of the tumor both before and post MRgFUS (white arrows), with a more pronounced enhancement on the post MRgFUS images. Post-contrast T1-weighted images in the axial plane also showed the enhancement in the brain tissue below the tumor along the path of the ultrasound beam (black arrow). Ktrans map from horizontal direction showed elevated Ktrans in the tumor prior to MRgFUS and an increase in Ktrans signal upon MRgFUS induction (white arrows). B showed the comparison of Ktrans values for Pre_FUS versus Post_FUS from the tumors of FUSX1 group. The Post_FUS Ktrans values increased significantly from Pre_FUS ones (p=0.03) (n=5 in each group)..

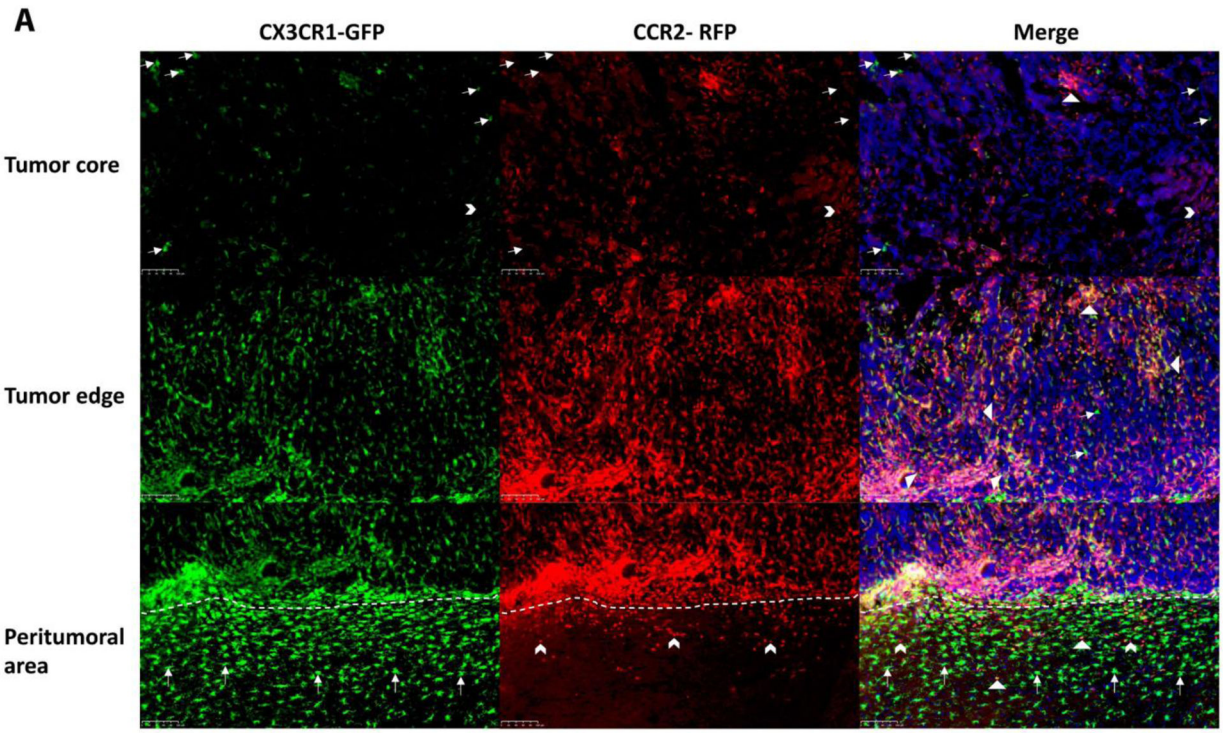

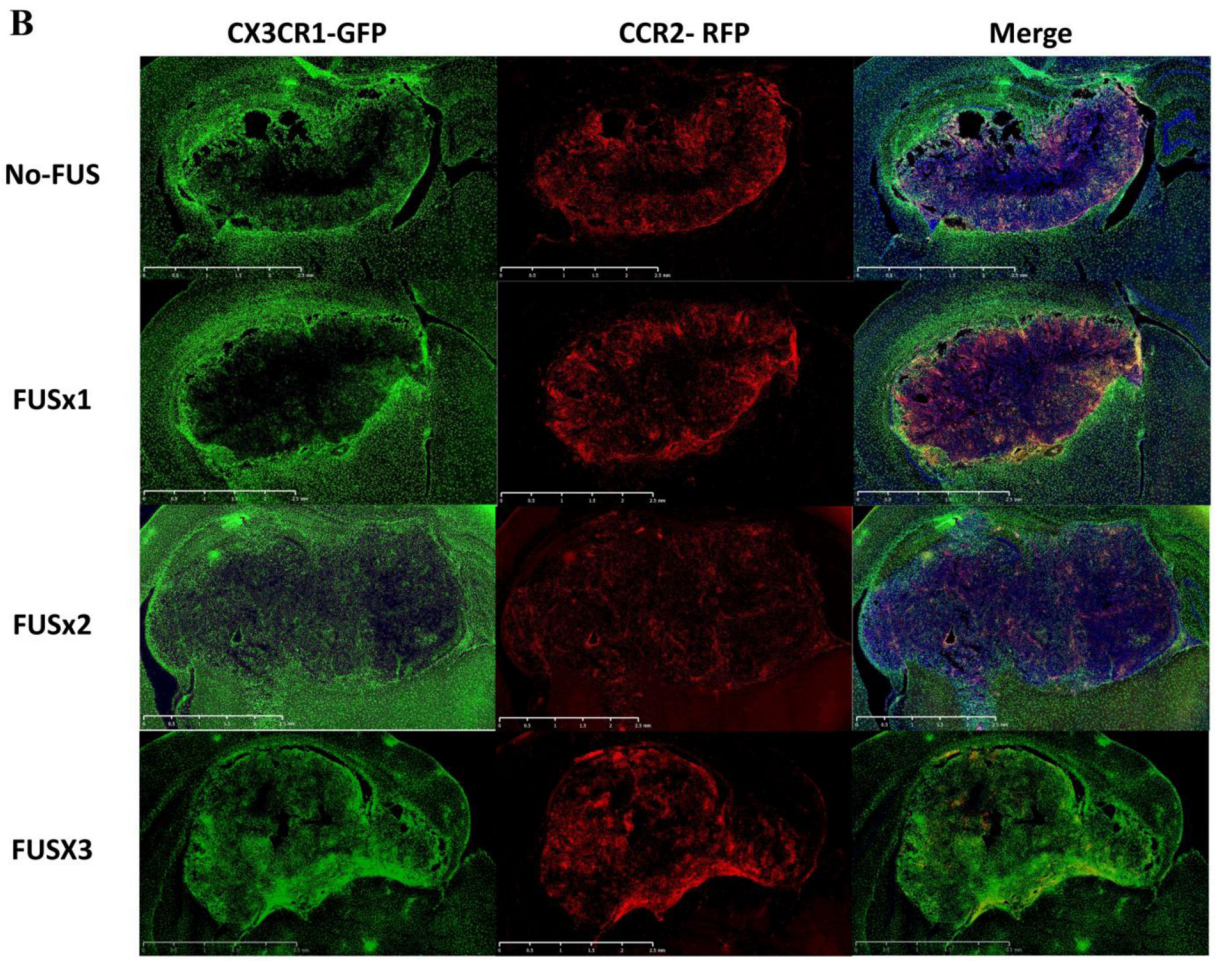

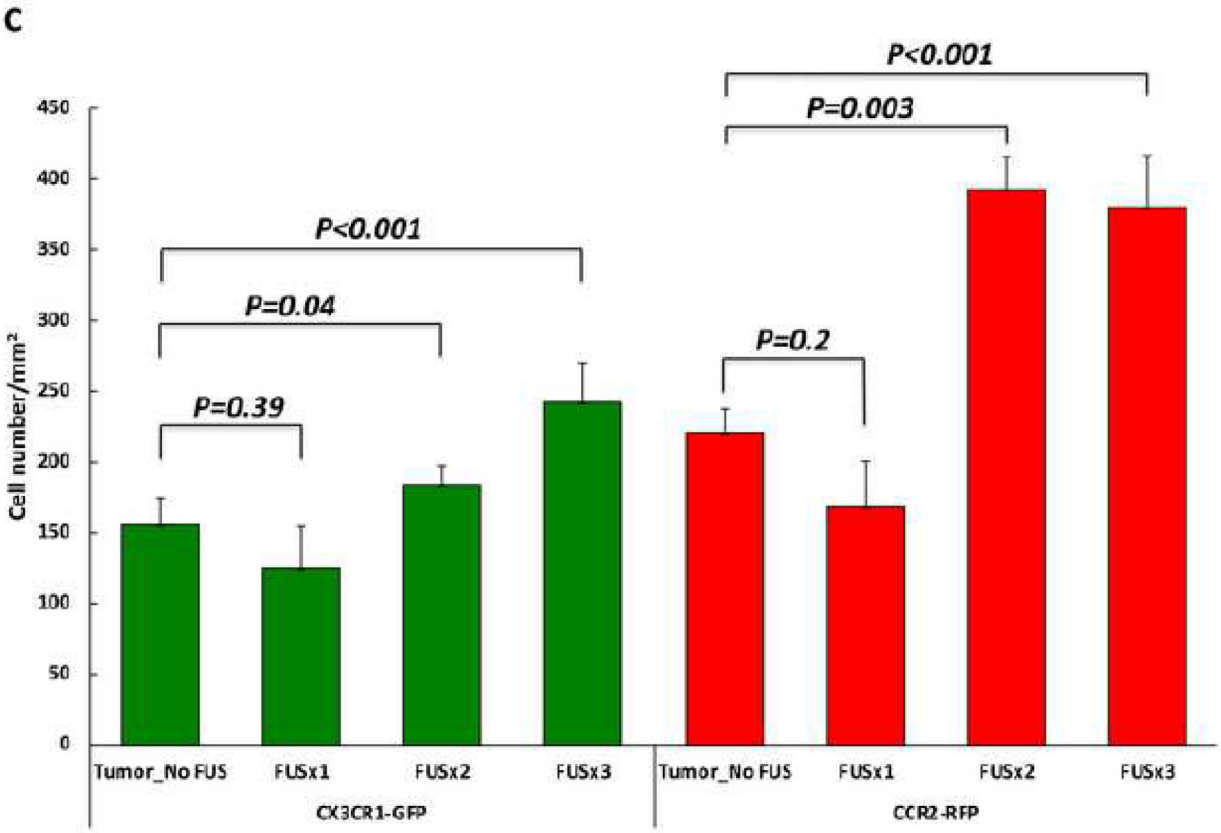

Figure 3. Infiltration of brain tumors by CCR2-RFP and CX3CR1-GFP immune cells.

A) Immunohistochemical staining for CX3CR1-GFP and CCR2-RFP cells is shown from an animal in the tumor-implanted group that did not receive MRgFUS. The fluorescent immune cells are mainly located at the edges of the tumor and in the peritumoral area with only a sparse distribution of cells in the core. Both in the tumor core and at the edges, dual-positive cells (First and second rows, triangles) are the predominant type, with occasional single-positive CX3CR1-GFP (First row, arrows) and CCR2-RFP (First and second rows, arrow heads) cells. In the peritumoral area (i.e. the areas below the dotted lines in the lower panels), there are more single-positive CX3CR1-GFP cells than single-positive CCR2-RFP cells, although dual-positive cells are seen in this area as well. B) Lower magnification images encompassing the tumor and peritumoral area for four experimental groups are shown. As described in A, stained cells in the Tumor_No FUS group exhibit stained cells toward the periphery of the tumor and in the peritumoral area. One session of FUS (FUSX1) did not appear to alter the distribution of cells. In contrast, two or three sessions of FUS (FUSX2 and FUSX3, respectively) resulted in increased numbers of immune cells infiltrating the tumor. C) Quantification of the cell density across the core and periphery of tumors demonstrated significantly greater infiltration of immune cells into tumors in animals receiving 2 or 3 sessions of FUS.

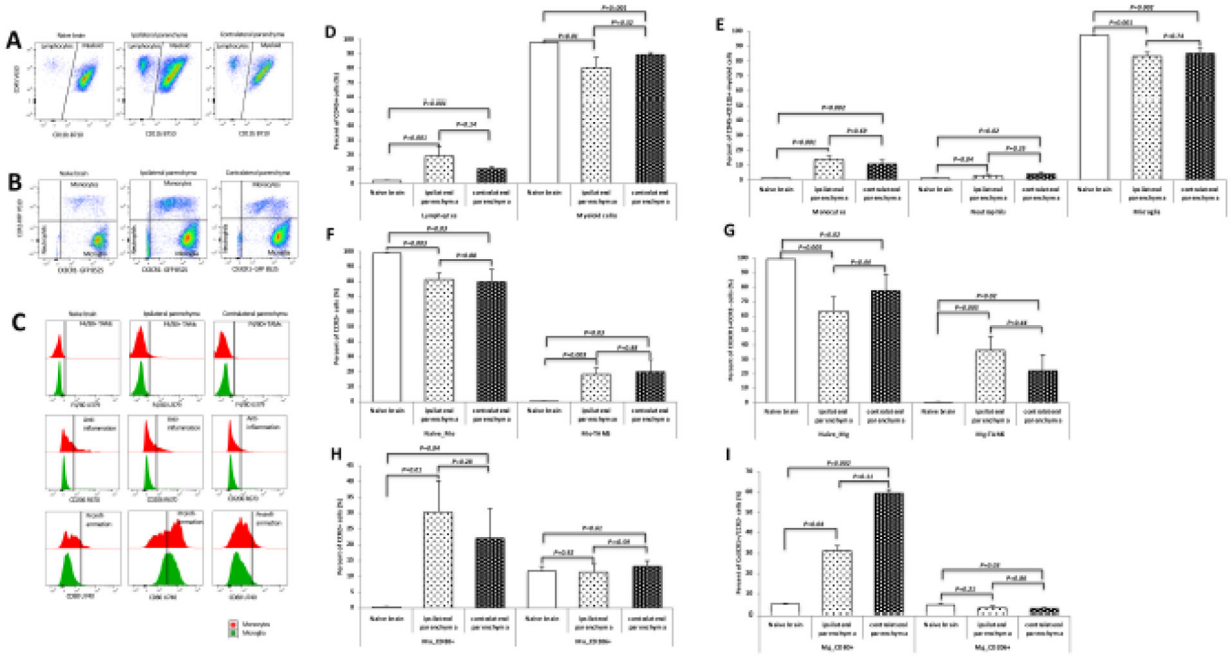

Figure 4. Immune micro-enviroment of naïve brain and the brain tissue implanted with GL26 glioma

A: Dot plots of the CD45+CD11b− lymphocytes and CD45+CD11b+ myeloid cells, Compared to the naïve brain, both ipsilateral and contralateral parenchyma of the brains allografted with tumor showed more lymphocytes.B: Dot plots gated on CX3CR1-GFP and CCR2-RFP from the CD45+CD11b+ myeloid cells. Monocytes were increased in both ipsilateral and contralateral parenchyma. C: Histogram plots from the staining of F4/80 showing the differentiation of monocytes and microglia identified from B; from the staining of CD80 and CD206 indicating the CD80+ proinflammation and CD206+ anti-inflammation polarization. D-I: Quantification of the immune cells identified from A, B, and C. The ipsilateral parenchyma showed more lymphocytes (p=0.001, D), monocytes(p=0.001, E), and neutrophils (p=0.04, E), and relatively lower proportion of microglia (p=0.001, E). The contralateral parenchyma displayed the same changes (lymphocytes: p=0.001, monocytes: p=0.002, neutrophils: P=0.02, microglia: p=0.002). The proportions of the immune cells between the ipsilateral and contralateral parenchyma did not show significant difference. Compared with naïve brain, the allografted parenchyma showed more monocyte-derived TAMs (ipsilateral parenchyma: p=0.003, contralateral parenchyma: p=0.03, F), and more microglia-derived TAMs (ipsilateral parenchyma: p=0.005, contralateral parenchyma: p=0.02, G). The bilateral parenchyma of the brain with GL26 glioma did not show significant difference in the differentiation of the monocytes (p=0.88) and microglia (p=0.44). H-I: There were more proinflammation CD80+ cells in monocytes (ipsilateral parenchyma: p=0.01, contralateral parenchyma: p=0.04) and microglia (ipsilateral parenchyma: p=0.04, contralateral parenchyma: p=0.002) of the ipsilateral and contralateral parenchyma compared with the naïve brain. The proportion of CD206+ cells in the contralateral parenchyma (p=0.03) was lower than the one from naïve brain. Abbreviation: naïve-Mo: naïve monocytes; Mo: monocyte; Mg: microglia; Mo-TAMs:

monocyte-derived tumor associated macrophages; naïve-Mg: maive microglia; Mg-TAMs: microglia-derived tumor associated macrophages.

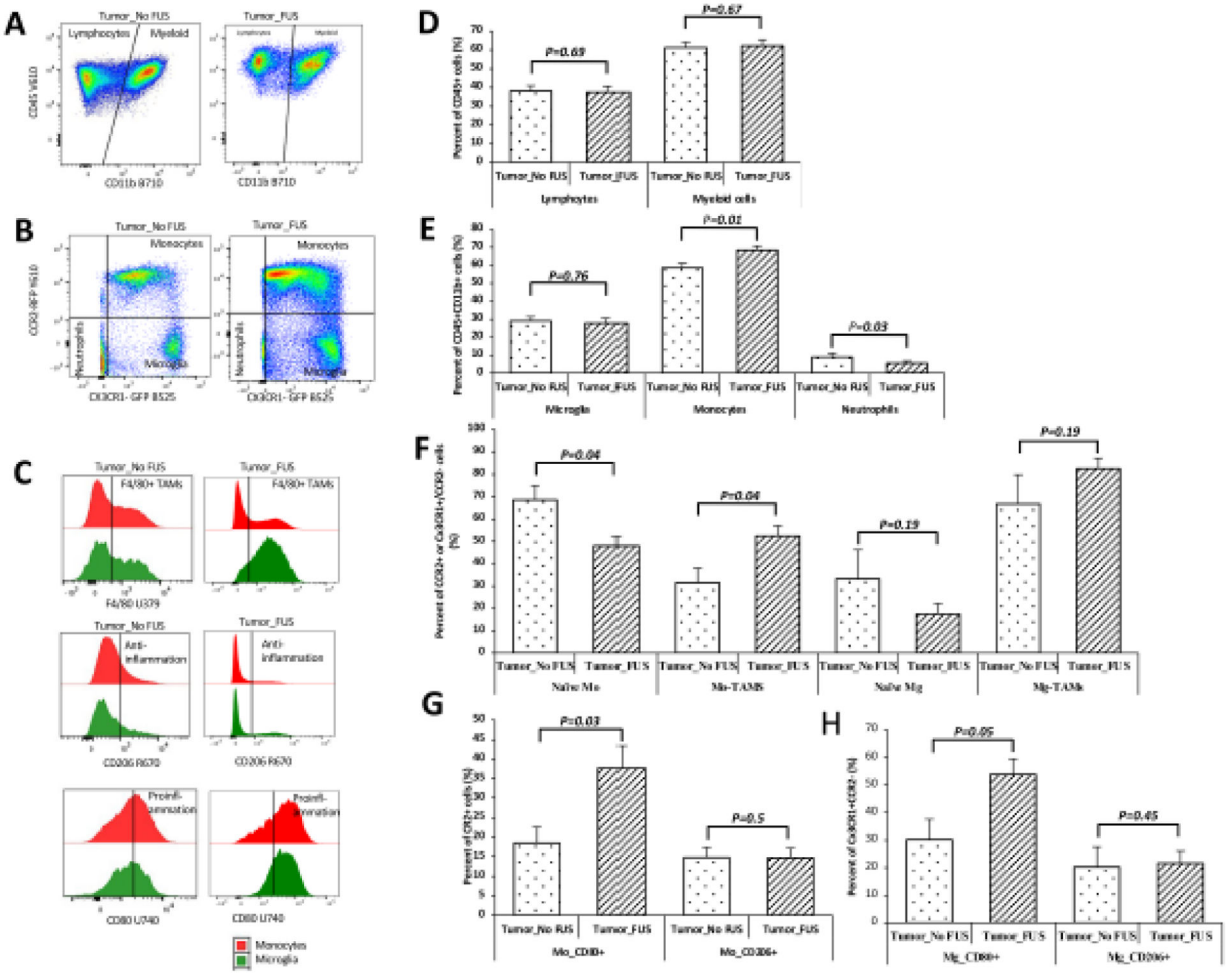

Figure 5. Effects of MRgFUS on the immune micro-enviroment of tumor tissue

A: Dot plots of the CD45+Cd11b− lymphocytes and CD45+CD11b+ myeloid cells. B: Dot plots of the cells gated on CX3CR1-GFP and CCR2-RFP from myeloid cells, the tumor treated with FUS showed more cells in the monocytes quardrant. C: Histograms of the monocytes and microglia cells identified through markers of F4/80, CD80, and CD206. D-H: Quantification of the cell populations identified from A, B, and C. The animals treated with MRgFUS showed increased monocytes ($p=0.01$) and decreased proportion of neutrophils ($p=0.03$) compared to the Tumor_No FUS group. The proportions of lymphcytes (p=0.69), myeloid cells (p=0.67), and microglia (p=0.76) did not show any significant difference between the gliomas from the Tumor_No FUS and Tumor_FUS groups (D and E). Tumor_FUS group showed more monocytes differentiation: higher proportion of monocytes-derived TAMs (p=0.04), whereas microglia did not show changes in differentiation (p=0.19) (F). In the tumors treated with FUS, there were more proinflammation CD80+ cells both in CCR2+ monocytes (p=0.03) and CX3CR1+CCR2− microglia cells (p=0.05). (G, H). Abbreviation: Abbreviation: naïve-Mo: naïve monocytes; Mo: monocyte; Mg: microglia; Mo-TAMs: monocyte-derived tumor

associated macrophages; naïve-Mg: maive microglia; Mg-TAMs: microglia-derived tumor associated macrophages.

Table 1.

Antibodies used in flowcytometry analysis

Epitope	Conjugate	Clone	Concentration (ul/test)	Supplier	Laser	Filter
CD45	Brilliant Violet 605	30-F11	1.5	BD Biosciences	405nm Violet	Vio3 (610/20)
CD11b	PerCP/Cy5.5	M1/70	5	BioLegend	488nm Blue	B2 (710/50)/550LP
F4/80	Brilliant Ultraviolet 395	T45-2342	1	BD Biosciences	355nm UV	UV-1 (379/29)
CD206	APC	C068C2	2.5	BioLegend	640nm Red	Red1 (670/30)
CD80	Brilliant Ultraviolet 737	16-10A1	2	BD Biosciences	355nm UV	UV-1 (740/30)